THE JOURNAL OF PHYSICAL CHEMISTRY A

Article

pubs.acs.org/JPCA

# Excited State Dynamics of Cold Protonated Cytosine Tautomers: Characterization of Charge Transfer, Intersystem Crossing, and Internal Conversion Processes

Michel Broquier,[†,‡] Satchin Soorkia,[†,‡] Gustavo Pino,[§] Claude Dedonder-Lardeux,[∥] Christophe Jouvet,[∥] and Gilles Grégoire*[,†,‡]

[†]Institut des Sciences Moléculaires d'Orsay (ISMO), CNRS, Univ. Paris-Sud, Université Paris-Saclay, F-91405 Orsay, France

[‡]Centre Laser de l'Université Paris-Sud (CLUPS/LUMAT), Univ. Paris-Sud, CNRS, IOGS, Université Paris-Saclay, F-91405 Orsay, France

[§]Instituto de Investigaciones en Físico Química de Córdoba (INFIQC) CONICET − UNC. Dpto. De Fisicoquímica − Facultad de Ciencias Químicas − Centro Láser de Ciencias Moleculares − Universidad Nacional de Córdoba, Ciudad Universitaria, X5000HUA Córdoba, Argentina

[∥]CNRS, Aix Marseille Université, PIIM UMR 7345, 13397 Marseille, France

Supporting Information

**ABSTRACT:** Charge transfer reactions are ubiquitous in chemical reactivity and often viewed as ultrafast processes. For DNA, femtochemistry has undeniably revealed the primary stage of the deactivation dynamics of the locally excited state following electronic excitation. We here demonstrate that the full time scale excited state dynamics can be followed up to milliseconds through an original pump−probe photodissociation scheme applied to cryogenic ion spectroscopy. Protonated cytosine is chosen as a benchmark system in which the locally excited $^1\pi\pi^*$ state decays in the femtosecond range toward long-lived charge transfer and triplet states with lifetimes ranging from microseconds to milliseconds, respectively. A three-step mechanism ($^1\pi\pi^* \rightarrow {}^1\mathrm{CT} \rightarrow {}^3\pi\pi^*$) is proposed where internal conversion from each state can occur leading ultimately to fragmentation in the ground electronic state.

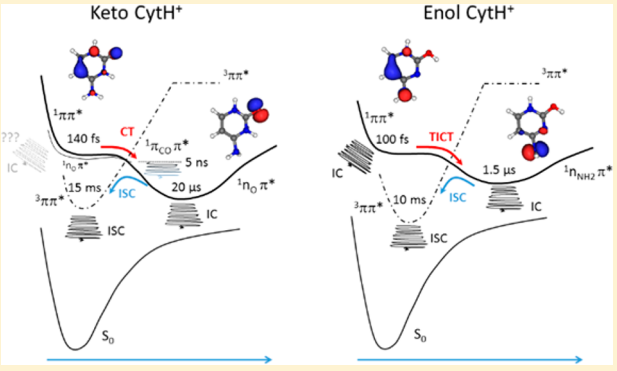


## 1. INTRODUCTION

Photochemical damage to DNA by UV absorption is one of the main causes of a possible mutagenic effect affecting the genetic material.[1] It has been suggested that excited state dynamics of these heterocycles has played a decisive role in the natural selection of the building blocks of life.[2] The excited state dynamics of DNA has indeed received much attention in the past thanks to the continuous advances in ultrafast spectroscopic techniques[3] and computational methodologies.[4,5] We shall refer the reader to the recent review articles (refs 4 and 5) to get an exhaustive list of condensed- and gas-phase studies on DNA photochemistry. The excited state photophysics of single nucleosides and nucleotides has been investigated in aqueous solution, pointing to an ultrafast, subpicosecond deactivation dynamics.[6,7] Such an ultrafast process is totally consistent with the very low fluorescence quantum yield of DNA nucleosides, about $10^{-4}$, measured through steady-state spectroscopy.[8] For cytosine (Cyt), the initially accepted mechanism is ascribed to direct relaxation to the ground electronic state through $^1\pi\pi^*/S_0$ conical intersection (CI) with low triplet quantum yield (<0.01).[9] However, significant solvent effects have been questioned in the radiationless decay by nucleobases, including relative stabilization of the bright $^1\pi\pi^*$ state compared to "dark" charge transfer (CT) states and fast intermolecular energy transfer to the solvent.[4,5,7,10] Besides, in single- and double-stranded oligonucleotides, lifetimes ranging from tens of picoseconds to nanoseconds have been reported.[11] These long-lived excited states have generally charge transfer character with very low fluorescence yield, making them difficult to detect in condensed phase through an ultrafast fluorescence up-conversion technique.[12]

From these seminal works, many gas phase studies have then been devoted to address the possible mechanism responsible for the ultrafast nonradiative process in DNA. Femtosecond time-resolved photoelectron[13] and mass-selected ionization spectroscopy[14−17] have been conducted on bare cytosine using

**Received:** June 30, 2017
**Revised:** July 28, 2017
**Published:** August 4, 2017







DOI: 10.1021/acs.jpca.7b06423
J. Phys. Chem. A 2017, 121, 6429−6439

different pump (from 300 to 260 nm) and probe wavelengths (800, 400, or 200 nm). Because of the lack of tautomer selection and the large excess energy brought by the fixed pump wavelength, the femtochemistry of Cyt was somehow difficult to rationalize. Overall, the femtosecond experiments have revealed multiexponential decay components with different weights and lifetimes ranging from 50 fs to a few ps plus a possible long time component that cannot be firmly assigned within the experimental time window. Besides, charge transfer and triplet states require a smaller probe wavelength than the one used for ionization from the $^1\pi\pi^*$, so the recorded ionic transients might be blind to the dynamics toward these low-lying states.

An active debate is still ongoing to decipher which reaction path should be the most important to access the ground state, either through direct 2-fold ($\pi\pi^*/S_0$) or 3-fold ($\pi\pi^*/n\pi^*/S_0$) degeneracy.[18,19] The picture is getting even more obscure when looking at the results of nonadiabatic dynamics[20−22] with an explicit account of spin−orbit coupling (SOC).[23] In almost all cases, the time constants extracted from the dynamical studies emphasize an ultrafast (subpicosecond) relaxation both to the ground state (independently of the two- or three-step mechanism) and to triplet states. These dynamics are always started following vertical excitation from the ground state, i.e., in the high energy region (about 0.5 eV of excess energy) of the PES. Thus, the calculated time constants and deactivation paths are relevant for comparison with the fs experiments (in which the excess energy is large) but do not apply to the deactivation from the vibrationless $^1\pi\pi^*$ minimum structure. Very recently, S. Blaser et al.[24] indeed measured the dependence of the $S_1$ ($^1\pi\pi^*$) state vibronic level lifetimes of keto Cyt through a picosecond pump−probe ionization scheme, revealing a lifetime of 730 ps at the band origin (BO), i.e., 1000 times longer than at higher energy. They also estimated the IC and ISC rates for keto Cyt for the low-lying vibronic levels of the $^1\pi\pi^*$ state.[25] IC rate constants are 20−50 times faster than the corresponding ISC rates that are predicted at about $10^9$ $s^{-1}$ but still way smaller than the ones calculated at larger excess energy. ISC was previously suggested for Cyt by E. Nir et al.[26] who observed a long time component of 290 ns in the two-color photoionization signal.

All of these experimental and theoretical results emphasize the need to study photochemical reaction in well controlled conditions. Cryogenic ion spectroscopy indeed fulfills such a requirement.[27,28] These spectroscopic studies rely on action spectroscopy, in which the absorption of a UV photon promotes the system in the excited state that ultimately leads to fragmentation.[29−31] Cryogenic ion spectroscopy allows deciphering the lowest energy conformers through their energy-resolved vibronic spectra. Besides, cold ion traps offer the unique opportunity of extending the experimental time window for time-resolved dynamics over seconds as compared to what can be done for neutral molecules streamed in supersonic expansion.[32−34]

Although the deactivation mechanisms in protonated nucleobases cannot be directly compared to those expected in neutrals, in both cases, the locally excited $^1\pi\pi^*$ state lies in close proximity to low-lying CT and triplet states. Since protonation occurs at the nitrogen site, the photodynamical process should be simplified as compared to neutral Cyt due to the absence of $n_N\pi^*$ state in keto $CytH^+$ (Chart 1). It is worth mentioning that the energy of the adiabatic transition to the bright $^1\pi\pi^*$ state of Cyt is not really affected by protonation, as

**Chart 1. Chemical Structure and Heavy Atom Numbering of the Keto $CytH^+$ (Protonation on $N_3$) and Enol $CytH^+$ (Protonation on $N_1$)**

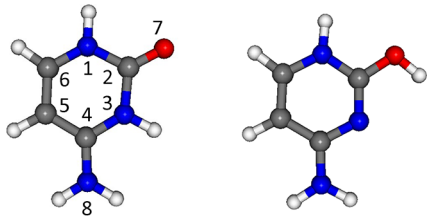


reported by Berdakin et al.[35] In the present paper, we report the full time scale excited state dynamics of protonated keto and enol cytosine ($CytH^+$) through pump−probe photofragmentation spectroscopy. The time-resolved dynamics has been followed over 10 decades, providing the complete deactivation process following electronic excitation. The lifetimes of the locally excited $^1\pi\pi^*$ state, charge transfer $^1n\pi^*$ states, and triplet $^3\pi\pi^*$ states have been determined for both tautomers in the 100 fs, $\mu$s, and ms time ranges, respectively. Geometry optimization and frequency calculations of the singlet and triplet states have been performed at the coupled-cluster CC2 level to assign the adiabatic excited state structures and to propose a general mechanism of deactivation to the ground state leading ultimately to fragmentation.

## 2. EXPERIMENTAL AND THEORETICAL METHODS

The experiments have been conducted at the Centre Laser of the Université Paris Sud (CLUPS) in Orsay. The experimental setup has been previously presented,[36] which comprises an electrospray ion source (ESI), a 3D-quadrupole ion trap QIT (Jordan TOF, Inc.) mounted on a cold head of a compressed helium cryostat that maintains the temperature around 10−15 K, and a linear time-of-flight mass spectrometer. The stored ions are thermalized through collisions with helium buffer gas introduced in the QIT by a pulsed valve (General valve, series 9) triggered a few ms before. The photodissociation UV laser, operated at 10 Hz, is shined into the trap after 40 ms to ensure complete cooling of the ions and pumping of the buffer gas. All of the ionic fragments and parent molecules are extracted and accelerated for mass analysis in a linear time-of-flight mass spectrometer and detected with microchannel plates (Z-Gap, Jordan TOF, Inc.). The resonant absorption of the UV laser is reflected by the observation of ionic fragments at lower masses. Action spectra are recorded by scanning the laser frequency and monitoring each ionic fragment signal normalized by the intensity of laser and the parent ion signal.

Three types of electronic spectroscopy have been performed: (i) the vibrationally resolved spectroscopy of the locally excited state through a one-color excitation scheme (UV only), (ii) the fragmentation kinetics of these fragment ions, and (iii) the time-resolved dynamics continuously monitored from picosecond to millisecond time scales through a two-color pump−probe excitation scheme. The combination of these experiments done on the same machine allows us to follow the complete dynamics in the excited and ground states on more than 10 decades:

In the ground state, the fragmentation kinetics following internal conversion is followed from hundreds of nanoseconds


DOI: 10.1021/acs.jpca.7b06423
J. Phys. Chem. A 2017, 121, 6429−6439

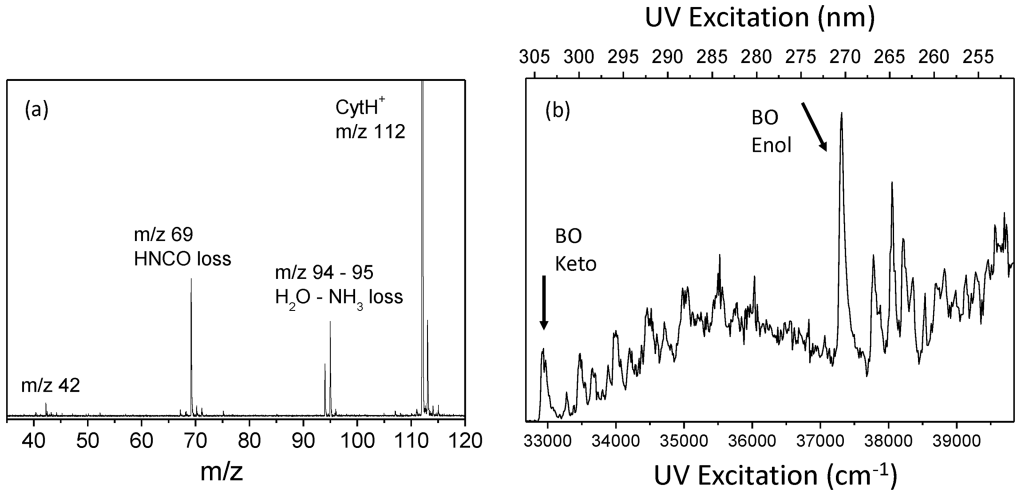


**Figure 1.** (a) UV photodissociation (one-color) mass spectrum of $CytH^+$. (b) Vibronic spectrum of $CytH^+$ from 306 to 250 nm averaged on the sum of the primary fragments. The two arrows indicate the band origin (BO) of the keto and enol tautomers.

to tens of milliseconds by delaying the extraction of the fragment ions from the photodissociation UV laser. The time resolution, on the order of one hundred of ns, is limited by the rise time of the high voltage pulser.

In the excited state: (1) The subpicosecond lifetime is deduced from the line width broadening of the vibronic spectrum (one-color). This is a perfectly effective measurement, since (i) the inhomogeneous broadening and the laser bandwidth are much smaller than the line width and (ii) the bare ions are cold without internal energy, avoiding spectral congestion due to low vibrational modes. (2) The picosecond time scale is investigated through a picosecond pump−probe photodissociation scheme using an optical delay line. (3) The longer time scale from tens of nanoseconds continuously up to tens of milliseconds is achieved in a pump−probe photodissociation scheme with two lasers electronically synchronized. More detail on the laser systems can be found in the Supporting Information.

*Ab initio* calculations have been done with the Turbomole program package[37] (v6.6) making use of the resolution-of-identity approximation.[38] Equilibrium geometries and vibrational frequencies in the ground electronic state $S_0$, singlet, and triplet excited states have been calculated at the coupled-cluster CC2 level[39] with the correlation-consistent polarized double-$\zeta$ aug-cc-pVDZ basis set augmented with diffuse functions.[40] True minima of the potential energy surface are systematically checked by looking at possible imaginary frequencies. In that case, in order to escape from the transition state minimum, the structure is distorted along the normal mode having a negative frequency (screwer module in Turbomole) and further optimized, leading to the stable structure without imaginary frequency.

## 3. RESULTS

**3.1. Vibronic Spectrum and Fragmentation Kinetics through a One-Color Excitation Scheme.** The UV photodissociation mass spectrum of protonated cytosine $CytH^+$ ($m/z$ 112) is reported in Figure 1a along with its electronic spectrum from 306 to 250 nm (Figure 1b). The electronic spectrum, averaged on all fragments ($m/z$ 95, 94 and 69), is similar to the one obtained with a nanosecond laser by Berdakin et al.[35] This electronic spectrum consists of two sets of vibronic progression reflecting the presence of two tautomers which have been previously assigned to the excitation of the locally excited $\pi\pi^*$ state that bears the oscillator strength for UV excitation of the keto and enol tautomers of $CytH^+$. The first intense transition at 32940 $cm^{-1}$ is the band origin (BO) of the $\pi\pi^*$ state of the keto form, while the enol tautomer has its BO at 37300 $cm^{-1}$, i.e., 0.54 eV to the blue. Broadening of the vibronic transition is clearly observed with a full width at half-maximum (fwhm) of 40 $cm^{-1}$ for the keto form and 55 $cm^{-1}$ for the enol tautomer, reflecting a short excited state lifetime in the range of 130 and 100 fs, respectively.[35,41]

Three main fragmentation channels are detected at $m/z$ 95 ($NH_3$ loss), $m/z$ 94 ($H_2O$ loss), and $m/z$ 69 (HNCO loss) for both $CytH^+$ tautomers. Their kinetics of fragmentation is the same for all ions. The evolution of the fragmentation time as a function of the excitation energy (UV) is reported in the Supporting Information (Figure SI1). The kinetics of fragmentation is 27 ± 2 $\mu$s at the BO of the keto tautomer and continuously decreases as the excitation energy increases down to less than 200 ns at the BO of the enol tautomer. Above this excess energy, the fragmentation kinetics is too fast to be accurately measured with our time resolution. These primary fragments are also observed through low-energy collision-induced dissociation.[42] Theoretical calculations indeed predict that ammonia loss and HNCO loss are produced after ring cleavage reaction of the $N_3-C_2$ bond[43] (see Chart 1 for atom labeling) through a transition state (TS8 in ref 43) which is the rate-determining step of the fragmentation process. We have calculated at the B3LYP/6-311++G(d,p) level the energetics following this path and have estimated its kinetics through RRKM modeling. The result reported in Figure SI1 closely matches the measured fragmentation times of $CytH^+$. Such simple modeling should be taken with care for a quantitative prediction; it nevertheless provides a qualitative picture of the kinetics of fragmentation. The main outcome is that photofragmentation must occur in the ground electronic state after internal conversion.

**3.2. Photodissociation Excited State Dynamics through a Two-Color Excitation Scheme.** In such an experiment,[32,36] the pump laser is tuned to a vibronic transition of the electronic spectrum, creating a population in a specific vibrational level of the locally excited state ($\pi\pi^*$) that evolves in


DOI: 10.1021/acs.jpca.7b06423
J. Phys. Chem. A 2017, 121, 6429−6439

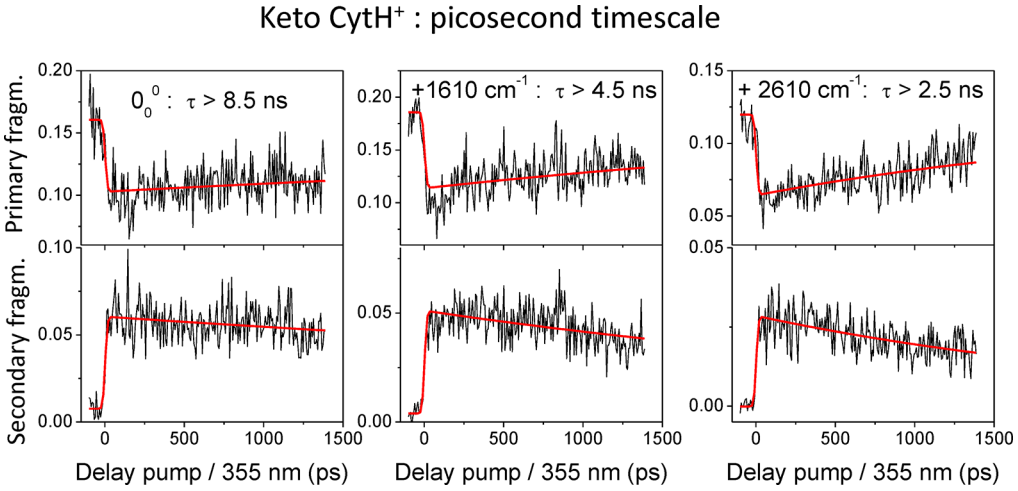


**Figure 2.** Photodissociation excited state dynamics averaged on the primary (top) and secondary (bottom) fragmentation channels as a function of the excess energy above the BO for keto CytH$^+$ for the first 1.5 ns.

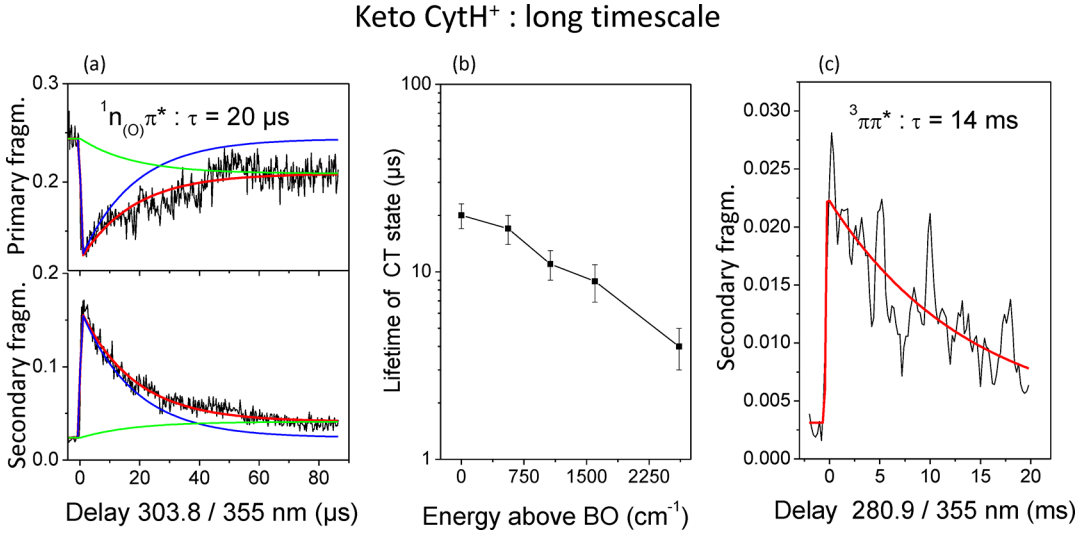


**Figure 3.** Photodissociation excited state dynamics for keto CytH$^+$ (a) at the BO for the first 100 $\mu$s. Full fit (red), exponential decay (blue), and exponential growth (green) functions with the same time constant $\tau$. (b) Evolution of the time constant $\tau$ recorded as a function of the excess energy above the BO. (c) Same as part a for the long time constant up to 20 ms.

time leading ultimately to dissociation of the parent molecule. It is worth mentioning that special attention has to be paid to the choice of the probe photon wavelength. The 355 nm probe laser used in this experiment fulfills the two following conditions: (i) Absorption can only occur from an electronic excited state of the parent ion to promote the initial population into a higher electronic excited state before internal conversion to the ground state occurs. It implies that "hot" ground electronic state does not absorb at 355 nm. This has been checked by using different probe wavelengths of the ps OPO laser from 450 to 600 nm without notable changes in the recorded transients. (ii) The probe laser cannot be absorbed by the primary fragment issued from the UV excitation. For CytH$^+$, all of the primary fragments ($m/z$ 95, 94, and 69) are closed-shell species with electronic transition in the UV range below 260 nm.

The time evolution of the initially excited state population (pump) can be monitored through absorption of the probe photon delayed in time as long as it induces a change in the fragmentation branching ratio. The variation of the fragmentation branching ratio upon absorption of the probe laser is related to the change in the fragmentation efficiency and/or opening of new fragmentation channels of the parent ions. The broadening of the vibronic bands of CytH$^+$ reveals a subpicosecond lifetime of the locally excited $\pi\pi^*$ state, which precludes to measure its dynamics with our picosecond laser (16 ps time resolution). Interestingly, we do observe a two-color photofragmentation signal, with a decrease of the fragmentation yield on the primary fragment ions at $m/z$ 95, 94, and 69 along with the concomitant increase of the fragmentation signal detected on secondary fragment channels at $m/z$ 68, 40 and a net increase of the fragmentation yield at $m/z$ 42 that was barely seen through one-color excitation (pump only). The absorption of a probe photon leads to an increase of the internal energy of the parent ion that can then undergo secondary fragmentation.

The fragmentation yield of CytH$^+$ through two-color is the same as that through one-color. This implies that the excited population (pump) that would initially decay to form the primary fragments is promoted to higher excited states (probe)


DOI: 10.1021/acs.jpca.7b06423
J. Phys. Chem. A 2017, 121, 6429−6439

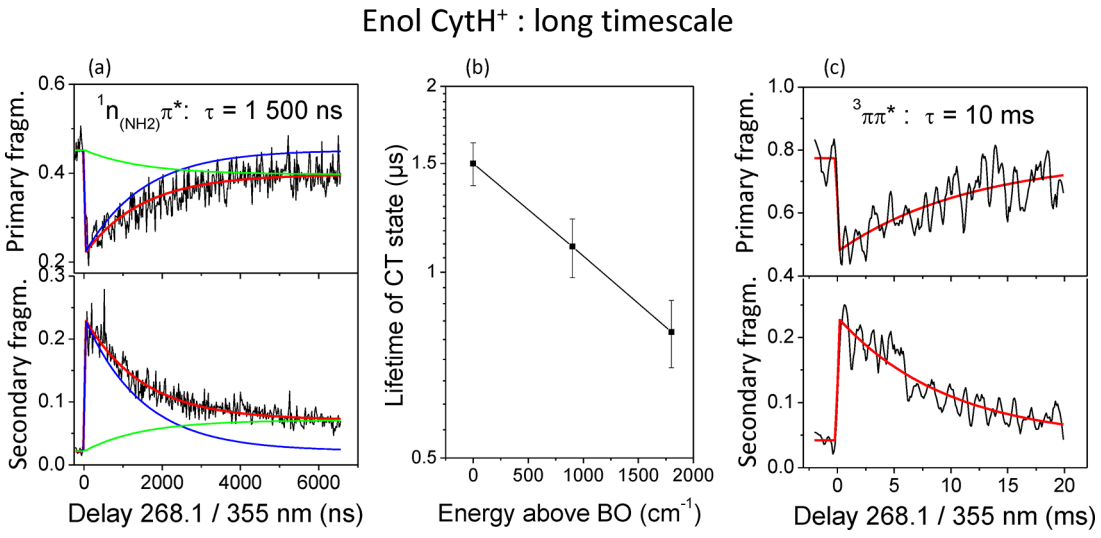


**Figure 4.** Photodissociation excited state dynamics for enol CytH$^+$ (a) at the BO for the first 7 $\mu$s. Full fit (red), exponential decay (blue), and exponential growth (green) functions with the same time constant $\tau$. (b) Evolution of the time constant $\tau$ recorded as a function of the excess energy above the BO. (c) Same as part a for the long time constant up to 20 ms.

leading to new fragments. The two-color signal has been recorded over 10 decades of pump−probe delays. Besides, the amplitude of the depleted signal on the primary fragments (UV only) is at least 50% of the total fragmentation yield. This definitively indicates that more than half of the initially created excited state population responsible for the one-color fragmentation signal evolves in the excited state potential energy surface (PES) for milliseconds. The analysis of the transients will reveal the lifetime of the electronic excited states responsible for the deactivation process following electronic excitation in CytH$^+$.

Independently of the time scale, the transients $S(t)$ recorded on each fragmentation channel are fitted by the sum of exponential decay and growth functions, starting at zero delay time $t_0$, with the same time constant $\tau$ but with different weights. As stated before, these transients do not contain a contribution from the hot electronic ground state populated after IC. This model fitting function indeed depicts a simple kinetics scheme in which the population of state 1 ($P_1$) decays with a time constant $\tau$ to a second excited state 2 (population $P_2$). Each population $P_i$ absorbs a 355 nm probe photon with an absorption cross section $\sigma_i$ that leads to specific ionic fragments (with $A_i = \sigma_i \times P_i$). This leads to eq 1

$$S(t) = A_0 + A_1 \times \exp^{-(t-t_0)/\tau} + A_2 \times (1 - \exp^{-(t-t_0)/\tau}) \quad (1)$$

in which $A_0$ is the background signal before time $t_0$ (UV photofragmentation only). Finally, this function is convoluted by a Gaussian function of width $l_0$ to account for the finite temporal profile of the laser beams (cross correlation of 16 ps for the picosecond lasers and 10 ns when using the nanosecond probe laser). For a given excitation energy associated with a time constant $\tau$, the only adjustable parameters are the amplitudes $A_i$.

The time evolution of the fragmentation yield on each fragmentation channel has been recorded for a set of pump wavelengths resonantly tuned to specific vibronic transitions for both keto (Figures 2 and 3) and enol (Figures 4 and SI2) tautomers. In all cases, the transients reported for the primary fragments are averages of the signals recorded at $m/z$ 95, 94, and 69, while the transients reported for the secondary fragments are averages of the signals recorded at $m/z$ 68, 42, and 40.

In Figure 2, the transient signals at several excitation wavelengths of the keto tautomer are monitored during the first 1.5 ns, the maximum time delay that can be reached with the optical delay line used with the two picosecond beams. It can be readily checked that the associated decays decrease with the excess energy and are in the nanosecond range. Since the time constants are longer than the maximum time delay, the time constants cannot be deduced confidently.

In Figure 3, the same transients are reported for a much longer time delay. Up to 100 $\mu$s (Figure 3a), the observed decay can be confidently fitted by eq 1 (red line) with a time constant $\tau$ of 20 ± 2 $\mu$s at the BO of the CytH$^+$ keto tautomer plus a long-lived component with lower intensity (green line) that stays constant on the 100 $\mu$s time scale. The evolution of the excited state lifetime $\tau$ (logarithm scale) with the excess energy above the BO of the keto conformer is reported in Figure 3b and exhibits a linear decrease down to 4 $\mu$s at 2500 cm$^{-1}$ of excess energy. Because of the constant signal recorded at the $\mu$s time scale, the time-resolved photofragmentation yield has been monitored on the millisecond time range (Figure 3c) and clearly exhibits a monoexponential decay signal with a time constant in the range of 14 ms. Here, the amplitude of the two-color signal is low and can only be detected on the background-free secondary fragments.

For the enol tautomer, the same procedure has been applied. The transients recorded on the 1.5 ns time scale do not exhibit any time evolution (step-like function, see Figure SI2) whatever the excitation wavelengths. On the $\mu$s time scale (Figure 4a), a time constant of 1.5 $\mu$s has been deduced from eq 1 at the BO plus a long-lived component (green line). The evolution of the excited state lifetime with the excess energy from the BO is reported in Figure 4b and shows a linear decrease (logarithm scale) as the excess energy increases down to 800 ns at 2000 cm$^{-1}$ above the BO. The transients recorded on the millisecond time scale (Figure 4c) show a monoexponential decay with a time constant of 10 ms at the BO and 5 ms 2000 cm$^{-1}$ above. For the enol tautomer, the amplitude of the two-color signal for



DOI: 10.1021/acs.jpca.7b06423
J. Phys. Chem. A 2017, 121, 6429−6439

the long delays is larger, which allows following the excited state lifetime on both the primary and secondary fragmentation channels.

The overall excited state dynamics of the keto and enol $CytH^+$ tautomers share similarities. The locally excited $\pi\pi^*$ state decays in the subpicosecond time scale, according to the spectral band broadening, toward a second excited state. For keto $CytH^+$, the lifetime of this excited state is in the range from 20 to 4 $\mu$s depending on the excess energy imparted in the $\pi\pi^*$ state. For enol $CytH^+$, the lifetime is reduced to 1.5 $\mu$s at the BO down to 800 ns 2000 $cm^{-1}$ above. As will be explained below, the states are assigned to charge transfer (CT) states of different electronic characters for the two tautomers. For both tautomers, a long-lived component with time constant in the 10 ms range is clearly seen, and will be assigned to the lifetime of the triplet state following intersystem crossing (ISC).

## 4. DISCUSSION

**4.1. Vertical Excited State Calculations.** *Ab initio* coupled-cluster (CC2/aug-cc-pVDZ) calculations have been performed on the electronic excited states of the keto and enol tautomers of $CytH^+$. Although many theoretical papers have been devoted to neutral cytosine,[5] a very few have been undertaken for the protonated analogue.[35,41] In the ground state, at this theoretical level, the most stable tautomer is the enol form while the keto tautomer is calculated 0.2 kcal/mol higher (E+ZPE). As already reported, both tautomers are detected through cryogenic ion spectroscopy with clearly distinguished band origins at 4.08 and 4.62 eV for the keto and enol tautomers, respectively. The assignment of the electronic transitions has been partially performed elsewhere.[41] In the present study, geometry optimizations and frequency calculations of the different electronic excited states, including the $\pi\pi^*$ state, charge transfer states, and triplet states, have been performed. The overall very good accuracy of the CC2 method to predict the adiabatic transition energies has already been discussed in detail[31,44] with an averaged error of about ±50 meV, which definitively allows a firm assignment of the electronic configuration of the different excited states and their optimized structures. However, such a monoconfigurational method cannot, by definition, treat the electronic couplings and curve crossings. The present calculations are thus relevant to provide the energies of the different minima of the excited state potential energy surface (PES).

The vertical excited state energies are reported in Table SI1 along with the corresponding molecular orbital (MO) representation. These vertical transitions and the ordering of the excited states are somehow meaningless for comparison with the experimental band origins. It nevertheless gives a rough picture of the electronic configuration of the excited states at the ground state optimized structure that will be used for further optimizations. In the ground electronic state, both keto and enol tautomers belong to the *Cs* point group in a planar geometry. For both tautomers, the first excited state corresponds to $\pi-\pi^*$ transition with high oscillator strength for optical excitation (A′). In the keto form, $S_2$ is a $n_O-\pi^*$ transition of A″ symmetry, 0.78 eV above the $S_1$ state, with very weak oscillator strength as expected for a charge transfer state. For the enol tautomer, the second excited state is also a $\pi\pi^*$ state, while the first charge transfer state ($S_3$) is calculated 0.73 eV above the bright $S_1$ state, and corresponds to a transition from the $n_{N3}$ lone pair orbital to the antibonding $\pi^*$ orbital of the aromatic ring.

**4.2. Adiabatic Excited State Calculations at the Franck–Condon Region (*Cs* Symmetry).** Geometry optimizations and frequency calculations of the locally excited $\pi\pi^*$ state and energy calculations of the charge transfer states ($n_O\pi^*$ for keto $CytH^+$ and $n_N\pi^*$ for enol $CytH^+$) at the optimized geometry of the $\pi\pi^*$ state have first been performed while keeping the *Cs* symmetry in order to stay close to the Franck–Condon active region (Table 1). For both $CytH^+$ tautomers, these excited state structures are saddle points of the PES, since one or more imaginary frequencies have been found. For the $\pi\pi^*$ state, it is totally consistent with the short excited state lifetimes deduced from the line broadening of the vibronic spectra. These modes are out-of-plane bending motions of the $NH_2$ and CH groups with calculated frequencies in the range from −40 to −400 $cm^{-1}$ (see Figure SI3). Therefore, the vibrationless adiabatic transitions cannot be accurately calculated but can be estimated by taking an average of the difference in zero point energy between the ground and excited states (−0.15 eV) that we have deduced in previous studies on related systems.[30,37] For both tautomers, the adiabatic transitions of the bright $\pi\pi^*$ state are then predicted within 80 meV or less to the experimental band origins, which is in line with the expected error of the CC2 method. It should be stressed here that both keto and enol tautomers can be univocally assigned through their calculated adiabatic energy transitions. Besides, there are some striking differences between the two tautomers.

**Table 1. Calculated Energy Transitions of Singlet and Triplet States of Keto and Enol $CytH^+$ (CC2/aug-cc-pVDZ) at the *Cs* $^1\pi\pi^*$ Optimized Structure (Franck–Condon Active Region)[a]**

| molecules | states | energy | $0_0^0$ exp |
|---|---|---|---|
| keto $CytH^+$ | $T_1$: $^3\pi\pi^*$ (A′) | 3.69 | |
| | $T_2$: $^3n_O\pi^*$ (A″) | 4.03 | |
| | $S_1$: $^1n_O\pi^*$ (A″) | 4.05 | |
| | **$S_2$: $^1\pi\pi^*$ (A′)** | 4.15 (**4.00**)[b] | **4.08** |
| enol $CytH^+$ | $T_1$: $^3\pi\pi^*$ (A′) | 3.89 | |
| | **$S_1$: $^1\pi\pi^*$ (A′)** | 4.79 (**4.64**)[b] | **4.62** |
| | $T_2$: $^3\pi\pi^*$ (A′) | 5.02 | |
| | $S_2$: $^1\pi\pi^*$ (A′) | 5.87 | |
| | $S_3$: $n_N\pi^*$ (A″) | 6.27 | |

[a]In bold, calculated $^1\pi\pi^*$ adiabatic energy compared to the experimental BO of the $^1\pi\pi^*$ state. All values in eV. [b]Adiabatic $0_0^0$ energy corrected by ΔZPE = −0.15 eV (see text).

For keto $CytH^+$, at the optimized structure of the bright $\pi\pi^*$ state (*Cs* symmetry), the $n_O\pi^*$ charge transfer state becomes the lowest energy minimum, 0.10 eV below (Figure 5). We have also calculated the energy of the triplet states at this structure (Table 1). The lowest triplet state is the $^3\pi\pi^*$ state, and $T_2$ is the $^3n_O\pi^*$, calculated 0.12 eV below the $^1\pi\pi^*$ state. Due to the unpaired electrons of the oxygen lone pair and $\pi$ orbital of the ring, the energies of the singlet and triplet charge transfer states are almost degenerated. Besides, we have optimized the structure of the $^1n_O\pi^*$ state while keeping the *Cs* symmetry. The state is further stabilized and lies 0.4 eV below the locally excited state.

For enol $CytH^+$, the situation is different, since, at the optimized structure of the singlet $^1\pi\pi^*$ (*Cs* symmetry), the corresponding $^3\pi\pi^*$ triplet state is the only state which lies below, at 0.9 eV. Since the optimized $^1n_N\pi^*$ charge transfer state ($S_3$ state, lowest A″ state) lies 0.38 eV above the $^1\pi\pi^*$, it is


DOI: 10.1021/acs.jpca.7b06423
J. Phys. Chem. A 2017, 121, 6429–6439

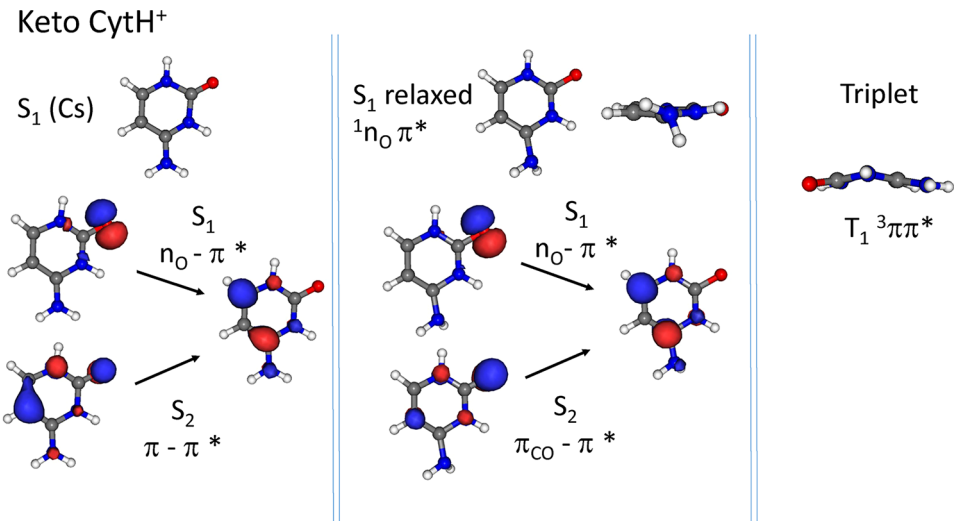


**Figure 5.** Excited state optimized structures of keto CytH$^+$ along with the corresponding frontier molecular orbitals involved in the different excited states.

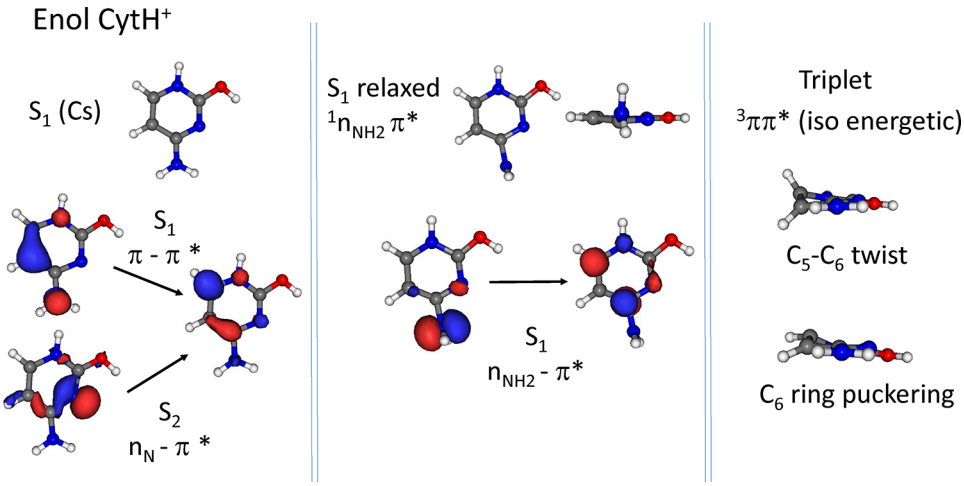


**Figure 6.** Excited state optimized structures of enol CytH$^+$ along with the corresponding frontier molecular orbitals involved in the different excited states.

not expected to play a role in the deactivation process in enol CytH$^+$. However, it should be pointed out that, for the $^1\pi\pi^*$ state, there is a non-negligible electron density on the $\pi$ orbital of the amino group, i.e., on the lone pair orbital of the nitrogen (Figure 6). This is exactly what is found in the case of protonated *p*-aminopyridine that undergoes a twisted intramolecular charge transfer (TICT) following electronic excitation of the $^1\pi\pi^*$ state.[33] As we will show below, the same process is proposed for enol CytH$^+$.

**4.3. Excited State Lifetimes of the Charge Transfer States and Triplet States.** In order to escape from these transition state structures, geometry optimizations without symmetry constraints have been performed (Table 2). In each case, the molecule is first distorted along the imaginary out-of-plane mode before being optimized.

For keto CytH$^+$, this leads to the adiabatic minimum with CT $n_O\pi^*$ electronic character, 0.56 eV below the calculated $\pi\pi^*$ transition at the FC active region (*Cs* symmetry). This CT state is the adiabatic $S_1$ state without imaginary frequency. The molecule has undergone a large structural change with a twist of the amino group out of the plane of the aromatic ring (Figure 5). The amino nitrogen has now a $sp^3$ hybridization with its lone pair pointing toward the protonated nitrogen. In this structure, the $S_2$ state is a $\pi_{CO}\pi^*$ transition, the electron density of the occupied orbital being mostly centered on the $\pi$ orbital of the carbonyl group, with much less electron density in the $\pi$ orbital of the aromatic ring. $S_2$, however, closely resembles the initial $\pi\pi^*$ with a partial charge transfer configuration.

**Table 2. Calculated Adiabatic Energy Transitions of Singlet and Triplet States of Keto and Enol CytH$^+$ (CC2/aug-cc-pVDZ) for Several Excited State Optimized Structures**[a]

| molecules (spin state) | optimized states | $0_0^0$ calc |
|---|---|---|
| keto (singlet) | $^1n_O\pi^*$ | 3.44 |
| | $^1\pi_{CO}\pi^*$ | 3.91 |
| keto (triplet) | $^3\pi\pi^*$ | 3.25 |
| | $^3n_O\pi^*$ | 3.43 |
| enol (singlet) | $^1n_{NH_2}\pi^*$ | 4.22 |
| enol (triplet) | $^3\pi\pi^*$ | 3.52 |
| | $^3\pi\pi^*$ | 3.56 |

[a]Energies corrected by the difference in zero point energy between the excited and ground states. All values in eV.



DOI: 10.1021/acs.jpca.7b06423
J. Phys. Chem. A 2017, 121, 6429−6439

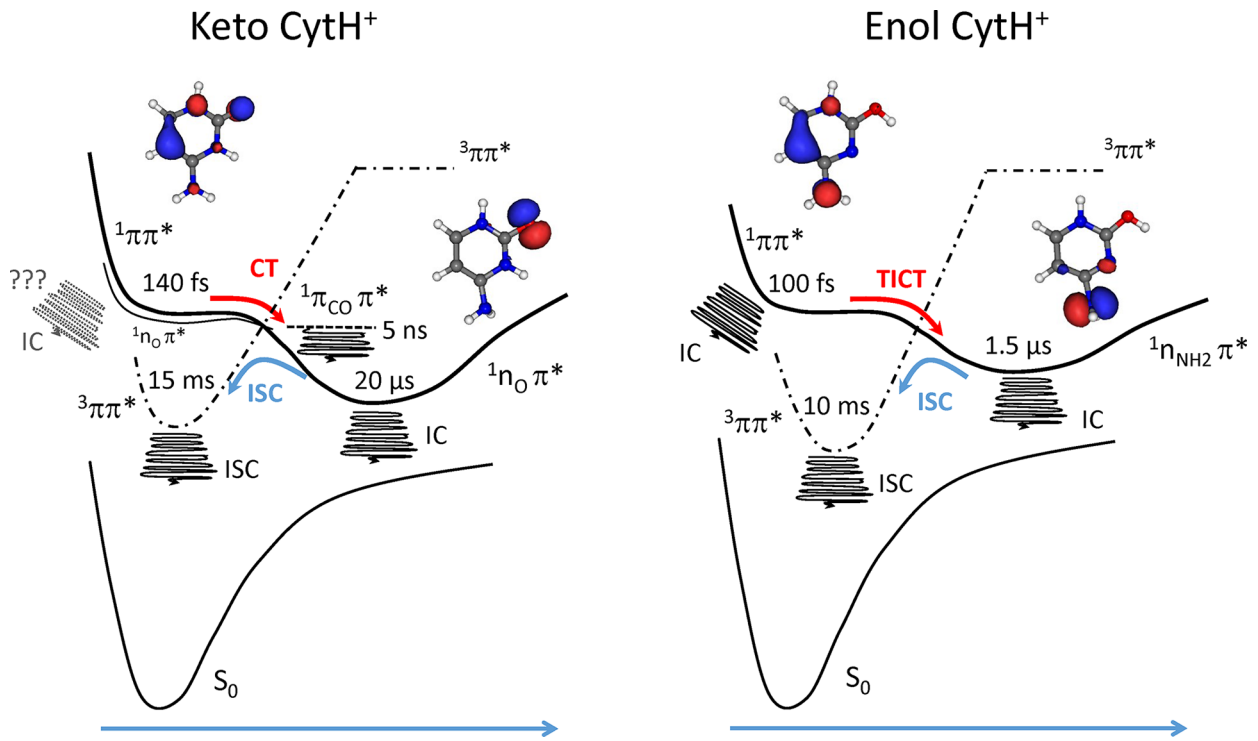


**Figure 7.** Schematic PES, excited state lifetimes, and proposed deactivation mechanisms to the ground state for keto and enol CytH$^+$.

Geometry optimization of the $S_2$ $\pi_{CO}\pi^*$ state does not lead to large structural change as compared to the optimized structure of the $n_O\pi^*$ state. $S_2$ $\pi_{CO}\pi^*$ is also a minimum of the PES, and its adiabatic energy (corrected by the ΔZPE) is calculated 0.09 eV below the adiabatic energy of the locally excited $\pi\pi^*$ state at the FC geometry. Finally, the $^3\pi\pi^*$ triplet state adiabatic energy is 0.2 eV below the singlet and triplet $n_O\pi^*$ states that are degenerated. The optimized structure of the $T_1$ $^3\pi\pi^*$ state leads to a slightly bent cytosine ring (along the $N_3-C_6$ axis) with the amino group twisted back to the plane of the aromatic ring (Figure 5), while the $T_2$ $^3n_O\pi^*$ retains the structure of the singlet state.

The barrierless process is totally consistent with the fs lifetime of the locally excited $^1\pi\pi^*$ state. In the course of the CT reaction, a two-step deactivation of the $\pi\pi^*$ state might occur. Experimentally, the nanosecond transient recorded for keto CytH$^+$ (Figure 2) might be assigned to the excited state lifetime of the $S_2$ $\pi_{CO}\pi^*$ state that decays to the adiabatic $S_1$ $n_O\pi^*$ state with lifetimes in the μs time range. The millisecond transient recorded for keto CytH$^+$ is assigned to the excited state lifetime of the $^3\pi\pi^*$ triplet state which is energetically accessible from the adiabatic minimum of the singlet PES ($^1n_o\pi^*$).

For the enol tautomer, the adiabatic minimum structure of the singlet excited state corresponds to the TICT state with the amino group twisted by 90° and bent out of the plane of the aromatic ring by 14° (Figure 6). This structure is a true minimum of the PES. This state has a charge transfer character, characterized by a transfer of the electronic density from the lone pair orbital of the $NH_2$ group to the $\pi^*$ orbital of the aromatic ring. The adiabatic transition energy of the $^1n_{NH_2}\pi^*$ state is calculated 0.42 eV below the calculated $\pi\pi^*$ band origin (Table 2). After UV excitation in the FC active region (*Cs* symmetry), the locally excited $\pi\pi^*$ state evolves into the CT $^1n_{NH_2}\pi^*$ in the course of the twist motion. It is worth mentioning that no other low-lying singlet excited state is predicted by the CC2 calculation, whereas low-lying triplet states are. The lowest triplet state is a $^3\pi\pi^*$ state, 0.7 eV below the degenerated singlet and triplet CT states.

The barrier free twisting motion leading to the TICT is compatible with the fs dynamics deduced from the broadening of the UV spectrum. The 1.5 μs decay recorded for enol CytH$^+$ (Figure 4) is assigned to the lifetime of this TICT state. The millisecond transient recorded for enol CytH$^+$ is assigned to the excited state lifetime of the triplet $^3\pi\pi^*$ state which is accessible from the adiabatic minimum of the PES (TICT state $^1n_{NH_2}\pi^*$). It should be stressed that the lifetimes of the TICT state and triplet state in enol CytH$^+$ are similar to those measured in protonated *p*-aminopyridine that also evolves to the TICT $^1n_{NH_2}\pi^*$ and $^3\pi\pi^*$ states.[33]

**4.4. Deactivation Processes in the Excited State Potential Energy Surface.** Both CytH$^+$ tautomers undergo ISC following initial electronic excitation of the $^1\pi\pi^*$ transition state which has a subpicosecond lifetime. Direct ISC from the locally excited $^1\pi\pi^*$ state to the lowest triplet $^3\pi\pi^*$ state would thus require very high singlet−triplet interactions in order to be effective with $k_{ISC} \approx 10^{13}$ s$^{-1}$. Such a high ISC rate constant for El-Sayed forbidden transition is unrealistic.[45] However, ISC is energetically and symmetry allowed according to El-Sayed rules[46] from CT states to the $^3\pi\pi^*$ state.

For enol CytH$^+$, at the FC region, the two lowest excited states are the $^1\pi\pi^*$ and $^3\pi\pi^*$ states, 0.9 eV below, so direct ISC is not thought to occur within the 100 fs lifetime of the locally excited state. The adiabatic singlet state, 0.4 eV below the $0_0^0$ transition, corresponds to the $^1n_{NH_2}\pi^*$ TICT state which has a 1.5 μs lifetime at the $0_0^0$ ($^1\pi\pi^*$) excitation energy. Populating the triplet $^3\pi\pi^*$ state from such a long-lived CT state does not require a high ISC rate. Thus, the proposed mechanism for the


DOI: 10.1021/acs.jpca.7b06423
J. Phys. Chem. A 2017, 121, 6429−6439

triplet formation in enol $CytH^+$ is a sequential process following $^1\pi\pi^* \rightarrow {}^1n_{NH_2}\pi^* \rightarrow {}^3\pi\pi^*$.

For keto $CytH^+$, we propose a similar sequential mechanism, the only difference being the ordering of the low excited states in the FC region. The bright $^1\pi\pi^*$ state is 0.4 eV above the adiabatic $S_1$ $^1n_O\pi^*$ state that is degenerated with its triplet state. Although $^1\pi\pi^* \rightarrow {}^3n_O\pi^*$ intersystem crossing would be allowed according to El-Sayed rules between states of different symmetries, the ISC rate should be larger than $10^{13}$ $s^{-1}$ to compete with the $^1\pi\pi^* \rightarrow {}^1n_O\pi^*$ process. Here again, since the $^1n_O\pi^*$ state has a 20 $\mu$s lifetime at the $0_0^0$ ($^1\pi\pi^*$) excitation energy, we suggest that the dominant ISC mechanism of keto $CytH^+$ is the sequential $^1\pi\pi^* \rightarrow {}^1\pi_{CO}\pi^* \rightarrow {}^1n_O\pi^* \rightarrow {}^3\pi\pi^*$ process.

It should be stressed that experimental evidence for the ISC process in neutral keto Cyt has already been reported by de Vries et al.[26] and Leutwyler et al.[25,47] In the latter studies, the authors quantify the rate constant $k_{ISC} \approx 10^9$ $s^{-1}$ for the direct $^1\pi\pi^*$ ($S_1$) $\rightarrow {}^3\pi\pi^*$ ($T_1$) process and a larger one, in agreement with El-Sayed rules, for the symmetry allowed mechanism $k_{ISC} \approx 10^{10}$ $s^{-1}$ for $^1\pi\pi^*$ ($S_1$) $\rightarrow {}^3n\pi^*$ ($T_2$). The unexpected high ISC rate for symmetry-forbidden transition ($S_1$–$T_1$) is caused by a substantial mixture of $^1n_O\pi^*$ character into the adiabatic $^1\pi\pi^*$ state which has a 730 ps lifetime at the band origin.[24] In $CytH^+$, the subpicosecond $^1\pi\pi^*$ lifetime clearly precludes the direct ISC process from the locally excited state to occur with a substantial quantum yield.

**4.5. Deactivation Pathways to the Ground State.** In $CytH^+$, fragmentation following UV excitation is energetically open only in the ground electronic state after internal conversion. There is no direct dissociation in the excited state, as found in protonated tryptophan[48,49] and aromatic amine,[30] for instance, where a dissociative $\pi\sigma^*$ excited state is coupled to the locally excited state. Therefore, the main questions are (i) from which states IC to the ground state occurs and (ii) can we quantify their rates?

Three different excited states are in play in the photofragmentation process of $CytH^+$ (see Figure 7): the $^1\pi\pi^*$ state which bears the strength for optical excitation and two dark CT and triplet $^3\pi\pi^*$ states. Each of these three states have quite different lifetimes, from sub-ps to $\mu$s up to ms, respectively, which allows unravelling their specific contributions in the deactivation process. Experimentally, the amplitude of the two-color signals indeed provides a qualitative information on the IC yield. When looking to the dynamics on the CT states ($\mu$s time scale), the depletion of the primary fragmentation yield through the absorption of the probe photon accounts for about half the UV only fragmentation signal. The absolute cross section absorption of the probe photon cannot be easily estimated, but it is unlikely that 100% of the initial excited state population is being promoted to higher excited states in the two-color scheme. Even within this hypothesis, we can confidently assume that at least the quantum yield for deactivation of the $^1\pi\pi^*$ to the CT states is larger than 0.5 for both tautomers.

For enol $CytH^+$, at the band origin, the fragmentation time recorded on the primary fragments is faster by almost 1 order of magnitude than the excited state lifetime of the CT state. This clearly indicates that part of the initially excited $\pi\pi^*$ state population returns to the ground state within 100 fs. For keto $CytH^+$, independently of the excess energy brought by the UV excitation, the recorded fragmentation times closely match the corresponding excited state dynamics, i.e., in the 20–4 $\mu$s time scale. RRKM calculations predict a similar time scale for the fragmentation in the ground state after internal conversion, so we cannot disentangle if the recorded kinetics of fragmentation is strictly the time-resolved dissociation or the convolution of the deactivation process from the CT state to the ground state leading to the dissociation.

Interestingly, a long time fragmentation kinetics has been recorded for both tautomers (Figure SI4), with a time constant in the range of 20 ms that is similar to the excited state lifetime of the triplet states. Because the fragmentation channels are the same independently of the time scale, the measured long fragmentation times simply reflect the deactivation dynamics of the triplet state through ISC to the ground state which thus dissociated within a few $\mu$s. The amplitude of the fragmentation yield at long time scale is at least twice the one recorded at the $\mu$s time scale, which reveals that more than 50% of the CT state population goes to the triplet state which then decays through ISC to the ground state, leading to the observed long time fragmentation events (Figure SI4). This proposed mechanism indeed suggests that, for enol $CytH^+$, ground state repopulation from the $^1\pi\pi^*$, CT, and triplet $^3\pi\pi^*$ states occurs. For keto $CytH^+$, ISC from the triplet $^3\pi\pi^*$ to the ground state accounts for 50% of the primary fragmentation signal. However, we cannot disentangle the IC process directly from the $^1\pi\pi^*$ state or from the CT state.

## 5. CONCLUSIONS

Using a combination of cryogenic ion photofragmentation spectroscopy and time-resolved excited state dynamics, the full time scale dynamics of excited protonated cytosine has been deciphered and the deactivation processes have been assigned through comparison with *ab initio* calculations at the CC2/aug-cc-pVDZ level including singlet, triplet excited state geometry optimizations and frequency calculations. For the keto and enol tautomers, the locally excited $\pi\pi^*$ state is a saddle point of the PES, in total agreement with the subpicosecond lifetime (about 150 fs) deduced from the line broadening of the vibronic spectrum. Although the deactivation mechanisms in protonated nucleobases cannot be directly compared to those expected in neutrals, in both cases, the locally excited $^1\pi\pi^*$ state lies in close proximity to CT and triplet states. It is worth mentioning that the energy of the adiabatic transition to the bright $^1\pi\pi^*$ state is not really affected by protonation, but its excited state lifetime is strongly reduced by 3 orders of magnitude from 700 ps to about 150 fs in keto Cyt. It is proposed that the $\pi\pi^*$ state decays without a barrier toward low-lying charge transfer states. These CT states, $^1n_O\pi^*$ for keto $CytH^+$ and $^1n_{NH_2}\pi^*$ for enol $CytH^+$, are the adiabatic minima of the excited state PES with 20 and 1.5 $\mu$s lifetimes at the BO of the $^1\pi\pi^*$ state of the keto and enol tautomers, respectively. A much longer lived component has been evidenced which has been assigned to the relaxation of the CT states through intersystem crossing to the lowest $^3\pi\pi^*$ triplet state with a lifetime in the order of 10 ms for both tautomers. For both $CytH^+$ tautomers, the fragmentation signals following UV excitation proceed from repopulation of the ground electronic state. In enol $CytH^+$, direct IC from the locally excited $^1\pi\pi^*$ has been evidenced and accounts for about half of the fragmentation signal. For keto $CytH^+$, IC to the ground state from either the $\pi\pi^*$ state or from the CT state cannot be disentangled from the experimental


DOI: 10.1021/acs.jpca.7b06423
J. Phys. Chem. A 2017, 121, 6429–6439

data, but ISC from the triplet $^3\pi\pi^*$ states accounts for about 50% of the fragmentation signal.

These results provide benchmark experimental data for the complete dynamics of protonated nucleobases followed over more than 10 decades which could thus be directly compared to multiconfigurational *ab initio* calculations in which vibronic couplings and singlet−triplet interactions can be calculated. Because protonated molecules have the same closed-shell electronic configuration as that in neutral analogues, these high-level calculations could be performed as well at the same cost. We believe that these experimental results could foster theoretical works to be done on protonated molecules. The energy- and time-resolved photodissociation experiment that we have developed provides the full time scale dynamics from the locally excited state toward the charge transfer states, the triplet states, and the ground state that ultimately leads to fragmentation. This unique experiment opens new areas for the precise knowledge of the photophysical processes in well-controlled molecular systems. The present results have focused on protonated cytosine and will be extended in the near future to the other nucleobases and nucleotides.

## ■ ASSOCIATED CONTENT

### Supporting Information

The Supporting Information is available free of charge on the ACS Publications website at DOI: 10.1021/acs.jpca.7b06423.

Additional results, table, and figures (PDF)

## ■ AUTHOR INFORMATION


### Corresponding Author

*E-mail: gilles.gregoire@u-psud.fr. Phone: (33) 1 69 15 31 03.

### ORCID

Gilles Grégoire: 0000-0002-8577-3621


### Notes

The authors declare no competing financial interest.

## ■ ACKNOWLEDGMENTS

This work has been conducted under the International Associated Laboratory LIA/LEMIR with financial support of CNRS GDR EMIE. We acknowledge the use of the computing facility clusters MésoLUM of the LUMAT federation (FRLUMAT 2764) and MAGI of the University Paris 13.

## ■ REFERENCES


(1) Schreier, W. J.; Gilch, P.; Zinth, W. Early Events of DNA Photodamage. *Annu. Rev. Phys. Chem.* **2015**, *66*, 497−519.

(2) Chen, I. A.; de Vries, M. S. From Underwear to Non-Equilibrium Thermodynamics: Physical Chemistry Informs the Origin of Life. *Phys. Chem. Chem. Phys.* **2016**, *18*, 20005−20006.

(3) Zewail, A. H. Femtochemistry: Atomic-Scale Dynamics of the Chemical Bond †. *J. Phys. Chem. A* **2000**, *104*, 5660−5694.

(4) Crespo-Hernández, C. E.; Cohen, B.; Hare, P. M.; Kohler, B. Ultrafast Excited-State Dynamics in Nucleic Acids. *Chem. Rev.* **2004**, *104*, 1977−2020.

(5) Improta, R.; Santoro, F.; Blancafort, L. Quantum Mechanical Studies on the Photophysics and the Photochemistry of Nucleic Acids and Nucleobases. *Chem. Rev.* **2016**, *116*, 3540−3593.

(6) Peon, J.; Zewail, A. H. DNA/RNA Nucleotides and Nucleosides: Direct Measurement of Excited-State Lifetimes by Femtosecond Fluorescence up-Conversion. *Chem. Phys. Lett.* **2001**, *348*, 255−262.

(7) Pecourt, J.-M. L.; Peon, J.; Kohler, B. DNA Excited-State Dynamics: Ultrafast Internal Conversion and Vibrational Cooling in a Series of Nucleosides. *J. Am. Chem. Soc.* **2001**, *123*, 10370−10378.

(8) Daniels, M.; Hauswirth, W. Fluorescence of the Purine and Pyrimidine Bases of the Nucleic Acids in Neutral Aqueous Solution at 300 K. *Science* **1971**, *171*, 675−677.

(9) Cadet, J.; Vigny, P. In *Bioorganic Photochemistry*; Morrison, H., Ed.; WILEY-VCH Verlag: New York, 1990; Vol. *1*, p 1.

(10) He, Y.; Wu, C.; Kong, W. Decay Pathways of Thymine and Methyl-Substituted Uracil and Thymine in the Gas Phase. *J. Phys. Chem. A* **2003**, *107*, 5145−5148.

(11) Georghiou, S.; Bradrick, T. D.; Philippetis, A.; Beechem, J. M. Large-Amplitude Picosecond Anisotropy Decay of the Intrinsic Fluorescence of Double-Stranded DNA. *Biophys. J.* **1996**, *70*, 1909−1922.

(12) Crespo-Hernández, C. E.; Cohen, B.; Kohler, B. Base Stacking Controls Excited-State Dynamics in A·T DNA. *Nature* **2005**, *436*, 1141−1144.

(13) Ullrich, S.; Schultz, T.; Zgierski, M. Z.; Stolow, A. Electronic Relaxation Dynamics in DNA and RNA Bases Studied by Time-Resolved Photoelectron Spectroscopy. *Phys. Chem. Chem. Phys.* **2004**, *6*, 2796.

(14) Kang, H.; Lee, K. T.; Jung, B.; Ko, Y. J.; Kim, S. K. Intrinsic Lifetimes of the Excited State of DNA and RNA Bases. *J. Am. Chem. Soc.* **2002**, *124*, 12958−12959.

(15) Canuel, C.; Mons, M.; Piuzzi, F.; Tardivel, B.; Dimicoli, I.; Elhanine, M. Excited States Dynamics of DNA and RNA Bases: Characterization of a Stepwise Deactivation Pathway in the Gas Phase. *J. Chem. Phys.* **2005**, *122*, 074316.

(16) Kosma, K.; Schröter, C.; Samoylova, E.; Hertel, I. V.; Schultz, T. Excited-State Dynamics of Cytosine Tautomers. *J. Am. Chem. Soc.* **2009**, *131*, 16939−16943.

(17) Ho, J.-W.; Yen, H.-C.; Chou, W.-K.; Weng, C.-N.; Cheng, L.-H.; Shi, H.-Q.; Lai, S.-H.; Cheng, P.-Y. Disentangling Intrinsic Ultrafast Excited-State Dynamics of Cytosine Tautomers. *J. Phys. Chem. A* **2011**, *115*, 8406−8418.

(18) Barbatti, M.; Aquino, A. J. A.; Szymczak, J. J.; Nachtigallová, D.; Lischka, H. Photodynamical Simulations of Cytosine: Characterization of the Ultrafast Bi-Exponential UV Deactivation. *Phys. Chem. Chem. Phys.* **2011**, *13*, 6145−6155.

(19) Nakayama, A.; Harabuchi, Y.; Yamazaki, S.; Taketsugu, T. Photophysics of Cytosine Tautomers: New Insights into the Nonradiative Decay Mechanisms from MS-CASPT2 Potential Energy Calculations and Excited-State Molecular Dynamics Simulations. *Phys. Chem. Chem. Phys.* **2013**, *15*, 12322−12339.

(20) Hudock, H. R.; Martínez, T. J. Excited-State Dynamics of Cytosine Reveal Multiple Intrinsic Subpicosecond Pathways. *ChemPhysChem* **2008**, *9*, 2486−2490.

(21) Lan, Z.; Fabiano, E.; Thiel, W. Photoinduced Nonadiabatic Dynamics of Pyrimidine Nucleobases: On-the-Fly Surface-Hopping Study with Semiempirical Methods. *J. Phys. Chem. B* **2009**, *113*, 3548−3555.

(22) Barbatti, M.; Borin, A. C.; Ullrich, S. In *Photoinduced Phenomena in Nucleid Acids*; Barbatti, M., Borin, A. C., Ullrich, S., Eds.; Springer International Publishing: Switzerland, 2014; pp 1−32.

(23) Mai, S.; Marquetand, P.; Richter, M.; Gonzalez-Vazquez, J.; Gonzalez, L. Singlet and Triplet Excited-State Dynamics Study of the Keto and Enol Tautomers of Cytosine. *ChemPhysChem* **2013**, *14*, 2920−2931.

(24) Blaser, S.; Trachsel, M. A.; Lobsiger, S.; Wiedmer, T.; Frey, H.-M.; Leutwyler, S. Gas-Phase Cytosine and Cytosine-N 1 -Derivatives Have 0.1−1 Ns Lifetimes Near the S 1 State Minimum. *J. Phys. Chem. Lett.* **2016**, *7*, 752−757.

(25) Lobsiger, S.; Etinski, M.; Blaser, S.; Frey, H.-M.; Marian, C.; Leutwyler, S. Intersystem Crossing Rates of S 1 State Keto-Amino Cytosine at Low Excess Energy. *J. Chem. Phys.* **2015**, *143*, 234301.

(26) Nir, E.; Müller, M.; Grace, L. I.; de Vries, M. S. REMPI Spectroscopy of Cytosine. *Chem. Phys. Lett.* **2002**, *355*, 59−64.

(27) Rizzo, T. R.; Stearns, J. A.; Boyarkin, O. V. Spectroscopic Studies of Cold, Gas-Phase Biomolecular Ions. *Int. Rev. Phys. Chem.* **2009**, *28*, 481−515.




DOI: 10.1021/acs.jpca.7b06423
J. Phys. Chem. A 2017, 121, 6429−6439

(28) Wolk, A. B.; Leavitt, C. M.; Garand, E.; Johnson, M. A. Cryogenic Ion Chemistry and Spectroscopy. *Acc. Chem. Res.* **2014**, *47*, 202−210.
(29) Gregoire, G.; Kang, H.; Dedonder-Lardeux, C.; Jouvet, C.; Desfrancois, C.; Onidas, D.; Lepere, V.; Fayeton, J. A. Statistical vs. Non-Statistical Deactivation Pathways in the UV Photo-Fragmentation of Protonated Tryptophan-Leucine Dipeptide. *Phys. Chem. Chem. Phys.* **2006**, *8*, 122−128.
(30) Féraud, G.; Broquier, M.; Dedonder-Lardeux, C.; Grégoire, G.; Soorkia, S.; Jouvet, C. Photofragmentation Spectroscopy of Cold Protonated Aromatic Amines in the Gas Phase. *Phys. Chem. Chem. Phys.* **2014**, *16*, 5250−5259.
(31) Féraud, G.; Broquier, M.; Dedonder, C.; Jouvet, C.; Grégoire, G.; Soorkia, S. Excited State Dynamics of Protonated Phenylalanine and Tyrosine: Photo-Induced Reactions Following Electronic Excitation. *J. Phys. Chem. A* **2015**, *119*, 5914−5924.
(32) Soorkia, S.; Broquier, M.; Grégoire, G. Conformer- and Mode-Specific Excited State Lifetimes of Cold Protonated Tyrosine Ions. *J. Phys. Chem. Lett.* **2014**, *5*, 4349−4355.
(33) Broquier, M.; Soorkia, S.; Dedonder-Lardeux, C.; Jouvet, C.; Theulé, P.; Grégoire, G. Twisted Intramolecular Charge Transfer in Protonated Amino Pyridine. *J. Phys. Chem. A* **2016**, *120*, 3797−3809.
(34) Soorkia, S.; Broquier, M.; Grégoire, G. Multiscale Excited State Lifetimes of Protonated Dimethyl Aminopyridines. *Phys. Chem. Chem. Phys.* **2016**, *18*, 23785−23794.
(35) Berdakin, M.; Féraud, G.; Dedonder-Lardeux, C.; Jouvet, C.; Pino, G. A. Excited States of Protonated DNA/RNA Bases. *Phys. Chem. Chem. Phys.* **2014**, *16*, 10643−10650.
(36) Broquier, M.; Soorkia, S.; Grégoire, G. A Comprehensive Study of Cold Protonated Tyramine: UV Photodissociation Experiments and Ab Initio Calculations. *Phys. Chem. Chem. Phys.* **2015**, *17*, 25854−25862.
(37) *TURBOMOLE V6.6*, a Development of University of Karlsruhe and Forschungszentrum Karlsruhe GmbH, 1989−2007, TURBOMOLE GmbH, since 2007; available from http://www.turbomole.com.
(38) Ahlrichs, R. Efficient Evaluation of Three-Center Two-Electron Integrals over Gaussian Functions. *Phys. Chem. Chem. Phys.* **2004**, *6*, 5119.
(39) Köhn, A.; Hättig, C. Analytic Gradients for Excited States in the Coupled-Cluster Model CC2 Employing the Resolution-of-the-Identity Approximation. *J. Chem. Phys.* **2003**, *119*, 5021.
(40) Kendall, R. A.; Dunning, T. H.; Harrison, R. J. Electron Affinities of the First-Row Atoms Revisited. Systematic Basis Sets and Wave Functions. *J. Chem. Phys.* **1992**, *96*, 6796.
(41) Pino, G. A.; Feraud, G.; Broquier, M.; Grégoire, G.; Soorkia, S.; Dedonder, C.; Jouvet, C. Non-Radiative Processes in Protonated Diazines, Pyrimidine Bases and an Aromatic Azine. *Phys. Chem. Chem. Phys.* **2016**, *18*, 20126−20134.
(42) Qian, M.; Yang, S.; Wu, H.; Majumdar, P.; Leigh, N.; Glaser, R. Ammonia Elimination from Protonated Nucleobases and Related Synthetic Substrates. *J. Am. Soc. Mass Spectrom.* **2007**, *18*, 2040−2057.
(43) Yao, C.; Tureček, F.; Polce, M. J.; Wesdemiotis, C. Proton and Hydrogen Atom Adducts to Cytosine. An Experimental and Computational Study. *Int. J. Mass Spectrom.* **2007**, *265*, 106−123.
(44) Winter, N. O. C.; Graf, N. K.; Leutwyler, S.; Hättig, C. Benchmarks for 0−0 Transitions of Aromatic Organic Molecules: DFT/B3LYP, ADC(2), CC2, SOS-CC2 and SCS-CC2 Compared to High-Resolution Gas-Phase Data. *Phys. Chem. Chem. Phys.* **2013**, *15*, 6623−6630.
(45) Tatchen, J.; Gilka, N.; Marian, C. M. Intersystem Crossing Driven by Vibronic Spin−orbit Coupling: A Case Study on Psoralen. *Phys. Chem. Chem. Phys.* **2007**, *9*, 5209−5221.
(46) El-Sayed, M. A. Spin—Orbit Coupling and the Radiationless Processes in Nitrogen Heterocyclics. *J. Chem. Phys.* **1963**, *38*, 2834−2838.
(47) Röttger, K.; Marroux, H. J. B.; Böhnke, H.; Morris, D. T. J.; Voice, A. T.; Temps, F.; Roberts, G. M.; Orr-Ewing, A. J. Probing the Excited State Relaxation Dynamics of Pyrimidine Nucleosides in Chloroform Solution. *Faraday Discuss.* **2016**, *194*, 683−708.
(48) Gregoire, G.; Lucas, B.; Barat, M.; Fayeton, J. A.; Dedonder-Lardeux, C.; Jouvet, C. UV Photoinduced Dynamics in Protonated Aromatic Amino Acid. *Eur. Phys. J. D* **2009**, *51*, 109−116.
(49) Gregoire, G.; Jouvet, C.; Dedonder, C.; Sobolewski, A. L. Ab Initio Study of the Excited-State Deactivation Pathways of Protonated Tryptophan and Tyrosine. *J. Am. Chem. Soc.* **2007**, *129*, 6223−6231.


DOI: 10.1021/acs.jpca.7b06423
*J. Phys. Chem. A* 2017, 121, 6429−6439